

Article

Microstructure of a V-Containing Cobalt Based Alloy Prepared by Mechanical Alloying and Hot Pressed Sintering

Niannian Li ¹, Fengshi Yin ^{2,*} and Liu Feng ^{3,*}

¹ School of Chemical Engineering, Shandong University of Technology, Zibo 255049, China; niannianli0708@163.com

² School of Mechanical Engineering, Shandong University of Technology, Zibo 255049, China

³ Analysis & Testing Center, Shandong University of Technology, Zibo 255049, China

* Correspondence: fsyin@sdut.edu.cn (F.Y.); willow-feng@163.com (L.F.); Tel.: +86-1360-533-1243 (F.Y.); +86-1358-949-8883 (L.F.)

Received: 8 March 2019; Accepted: 16 April 2019; Published: 22 April 2019



Abstract: In this paper, a bulk V-containing cobalt-based alloy with high chromium and tungsten contents was prepared by mechanical alloying and hot pressed sintering using Co, Cr, W, Ni, V and C pure element powders. XRD, SEM, TEM and Vickers hardness tests were employed to characterize the microstructure and mechanical properties of the mechanical alloyed powders and hot pressed bulk cobalt-based alloy. The results show that all elements can be mixed uniformly and that the Co, Cr, and Ni elements were made into an amorphous state after 10 h ball milling in a high energy ball miller. The microstructure of the prepared bulk alloy was composed of a γ -Co matrix with a large number of nano-twins and fine $M_{23}C_6$ and $M_{12}C$ carbide particles well-distributed in the alloy. The V element was mainly distributed in $M_{23}C_6$ -type carbide and no V-rich MC-type carbide was found in the microstructure. The prepared alloy had a high hardness of 960 ± 9.2 HV and good a fracture toughness K_{Ic} of about 10.5 ± 0.46 MPa·m^{1/2}. The microstructure formation and strengthening mechanisms of the prepared cobalt-based alloy are discussed.

Keywords: cobalt-based alloy; mechanical alloying; hot pressed sintering; microstructure

1. Introduction

Stellite alloys, a kind of Co-based alloys, are very important in the development of science, technology, and the progress of industry. They are mainly composed of carbon, cobalt, chromium, tungsten, molybdenum, etc. Metal carbides formed in the alloy are used as hard phases and Co as the matrix bonding phase [1,2]. Stellite alloys are widely used industries such as aerospace, nuclear, mining machinery, and material machining due to their characteristics of wear-resistance, high temperature resistance, high strength, high hardness, and a certain toughness. In order to further increase the wear-resistant properties, Triballoy alloy, another kind of Co-based alloys, which contains a large volume fraction of intermetallic Laves phases in γ -Co matrix, has been developed [3,4]. It is the presence of this large volume fraction of Laves phases that enables these materials to resist wear under poor or unlubricated conditions.

Typically, cobalt-based alloys are prepared by casting or powder metallurgy technology. The casting process is simple in terms of the technology needed and low in cost, but the size and distribution of carbides are strongly dependent on the casting temperature of the melt, cooling rate, and thermal treatment condition, which must be strictly controlled to avoid defects such as macro-segregation, micro-segregation, porosity, solidification shrinkage, and second phase inclusions [5,6]. Cobalt-based alloys can be also manufactured by powder metallurgy process using pre-alloyed powders [7,8].

However, chemical element segregation and oxidation will occur on the surface of the pre-alloyed powders, which introduces the prior particle boundary (PPB), and therefore, decreases the mechanical properties of the final powder metallurgy product [9]. Mechanical alloying (MA) [10–12] and hot pressed sintering, as another powder metallurgy technology, have the potential to shorten the whole preparing period and produce bulk materials with a uniform fine-grained microstructure. The as-prepared materials exhibit excellent properties such as high density, good hot workability and improved mechanical properties.

It is well known that vanadium is a strong carbide-forming element and vanadium-containing high speed steel W18Cr4V has a good wear-resistant property. However, there is no report about the effect of vanadium on cobalt-based alloys. Berthod [13] reported a TiC carbide containing cobalt-based alloy. In this work, based on the Stellite alloys, we designed a novel vanadium-containing cobalt-based alloy with high chromium and tungsten contents. The alloy was prepared using MA and vacuum hot pressed sintering methods aiming to further increase the wear-resistant property of cobalt-based alloy. The microstructure and mechanical properties of the mechanically alloyed powders and hot pressed bulk cobalt-based alloy was characterized.

2. Materials and Methods

The cobalt-based alloy with a nominal composition of Co-32.4%, Cr-32%, W-25%, Ni-5%, V-5%, and C-0.6% (in wt. %) was prepared by mechanical alloying and hot pressing using pure element powders of Co, Cr, W, Ni, V, and C. The purity of these elemental powders was greater than 99.5%. The process of mechanical alloying was carried out in a high energy ball mill (SPEX8000D, SPEX SamplePrep, Metuchen, NJ, USA) using a stainless-steel vial and stainless-steel balls of 7 mm in diameter. The ratio of ball to powder was 10:1 in weight. The 5 wt. % ethanol was used as the process control agent during the ball milling process. The volume of the vial was 56 mL. A 10 g mixture of the powders with the stainless-steel balls was charged into the stainless-steel vial under high pure argon atmosphere. The ball milled powders were put into a graphite mold and sintered in a vacuum hot press sintering furnace (ZRY-30L, Jinzhou Hangxing Vacuum Equipment Co., Ltd., Jinzhou, China). After the furnace was evacuated using a vacuum pump to 10 Pa and then heated to 1200 °C at a heating rate of 4 °C/min, the ball milled powders were sintered at a pressure of 60 MPa for 20 min and cooled in the furnace. The ball milled powders and hot pressed bulk sample were examined by X-ray diffraction with Cu K α radiation (XRD, Bruker AXS D8 Advance, Bruker AXS GmbH, Karlsruhe, Germany), a scanning electron microscope (SEM, FEI Quanta 250, FEI, Hillsboro, OR, USA), and a transmission electron microscope (TEM, FEI Tecnai G2 F20, FEI, Hillsboro, OR, USA) equipped with energy dispersive X-ray spectrometry (EDS, EDAX Apollo) and a scanning transmission electron microscope mode (STEM). Quantitative metallography was used to measure the volume fraction and particle size of various phases in the microstructures of the obtained alloy. The TEM samples were prepared by an ion thinning instrument (Gatan 695.C, Gatan, Inc., Pleasanton, CA, USA). The hardness of the hot pressed bulk sample was measured by a Vickers hardness tester (Laizhou Huayin Testing Instrument Co., Ltd., Laizhou, China) using a 5 kgf load. Fracture toughness was determined according to the hardness indentation method. Five measurements were used to calculate average value of hardness and toughness.

3. Results

Figure 1 shows the XRD patterns of the powders ball milled with various time. It can be seen that at the initial state, the diffraction peaks of Co, Cr, W, and Ni are clearly shown in the pattern, while the corresponding diffraction peaks of C and V were not present due to their low content. The diffraction intensity of all elements decreased gradually with the milling time. The diffraction peaks of Co, Cr, and Ni elements almost disappear except for the W element after 10 h milling. No obvious change was seen upon further milling for up to 30 h, but peak broadening of W elements was observed. The disappearance of the diffraction peaks of Co, Cr, and Ni elements indicates that these element

powders were transformed into an amorphous state. The XRD peak broadening reveals that the W powders had been transformed into a nanocrystalline state. The crystallite size of the W powders after milling 10 and 30 h, estimated using the Scherrer formula [14], was found to be approximately 25 and 17 nm, respectively.

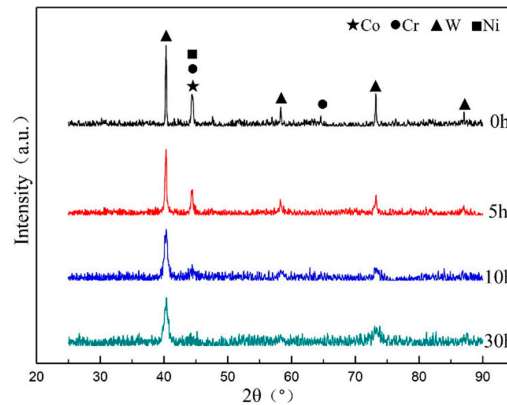


Figure 1. X-ray diffraction patterns of the powders ball milled for different time.

The morphology and micro-structural details of the milled powders were investigated by SEM. Figure 2 shows the SEM images for the powders ball milled for 10 h. The milled powders had an irregular morphology with a size below 15 μm . A local amplified back-scattered electron (BSE) image (Figure 2b) of one particle shows that some white particles about 30 nm in size are distributed uniformly in the powders. According to the XRD results of the milled powders (Figure 1), the white particles were deduced to be W phase. The element mapping image (Figure 2c) of EDS reveals that all elements had been mixed uniformly after 10 h ball milling.

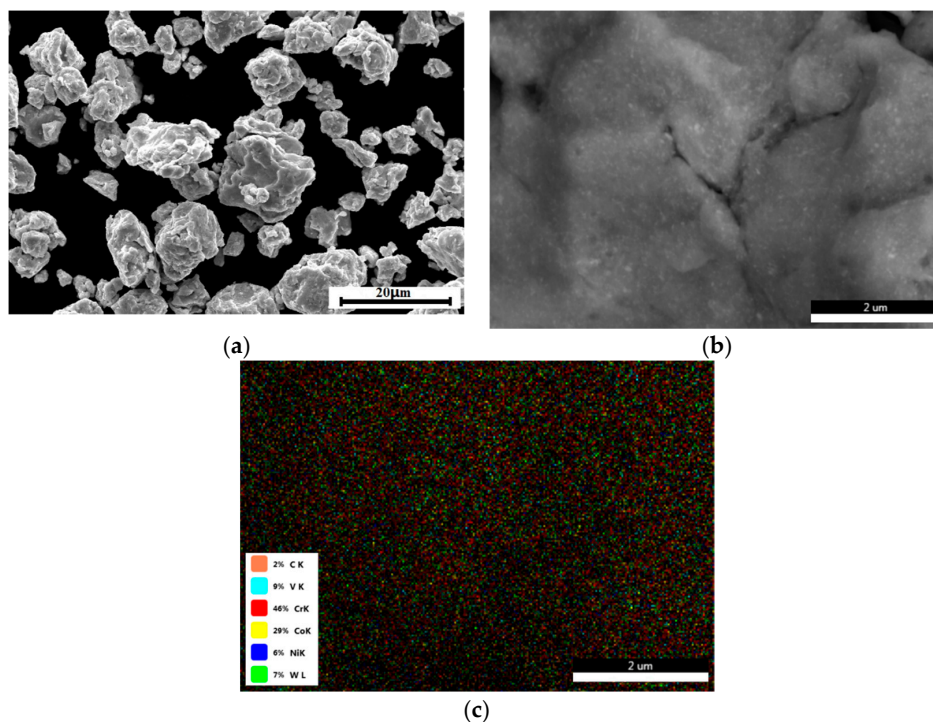


Figure 2. SEM images of the cobalt-based alloy powders after milling for 10 h, (a) morphology of the milled powders, (b) back-scattered electron (BSE) image of one particle, and (c) element mapping image of energy dispersive X-ray spectrometry (EDS) results.

The cobalt-based alloy powders milled for 10 h were selected for vacuum hot pressed sintering in the subsequent experiment. Figure 3 is the SEM-BSE image of the obtained bulk cobalt-based alloy showing that there were three kinds of phases in the alloy according to the contrast, i.e., bright, grey, and dark phases. XRD results (Figure 4) of the obtained bulk cobalt-based alloy show that these three phases were $M_{12}C$ (Co_6W_6C , JCPDS 22-0597), γ -Co (JCPDS 15-0806) matrix, and $M_{23}C_6$ ($Cr_{23}C_6$, JCPDS 85-01281), respectively, all of which had a cubic structure. According to the XRD results, the lattice constants of $M_{12}C$, γ -Co and $M_{23}C_6$ were 1.0922, 0.3552, and 1.0657 nm, respectively. No PPBs were found (Figure 3) in the prepared alloy by hot pressed sintering using mechanical alloyed powders. Figure 5 is STEM high-angle annular dark field (HAADF) image and selected area electron diffraction (SAED) patterns of the phases with different morphology and contrast. Both the STEM-HAADF and SEM-BSE images are atomic number contrast (Z-contrast) images, the γ -Co matrix, M_6C , and $M_{23}C_6$ phases have similar contrast in Figures 3 and 5. Table 1 summarizes the STEM-EDS results and identified phases by SAED patterns for the phases labeled in Figure 5a. Fe in EDS results would have been introduced from stainless-steel vial and balls during mechanical alloying process. According to the results mentioned above, we can conclude that the bright phase was W-containing $M_{12}C$ carbide in which lots of Cr and V atoms dissolved, the grey phase is the γ -Co matrix, and the dark phase was Cr and V-rich $M_{23}C_6$ carbide. The V element was mainly distributed in $M_{23}C_6$ -type carbide and no V-rich MC-type (M indicates metal elements) carbide was found in the obtained alloy. The $M_{12}C$ -type carbide particles had a size of about 1 μm dispersed in the γ -Co matrix. Some coarse $M_{23}C_6$ -type carbide particles have a strip-like shape with about 1 μm in length dispersed in the γ -Co matrix and some fine $M_{23}C_6$ -type carbide particles with about 200 nm in length present within both the γ -Co matrix and $M_{12}C$ -type carbide. The volume fraction of $M_{12}C$ and $M_{23}C_6$ phases were determined to be about 19.4% and 11.95%, respectively, by using quantitative metallography.

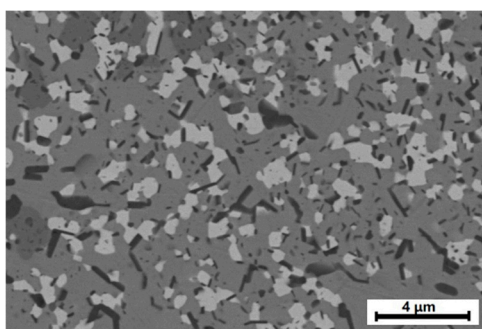


Figure 3. SEM back-scattered electron image of the obtained bulk cobalt-based alloy.

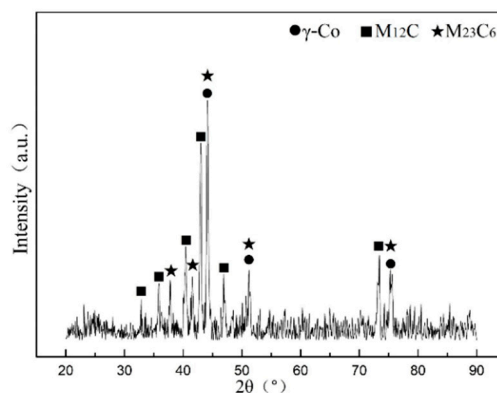


Figure 4. XRD result of the obtained bulk cobalt-based alloy.

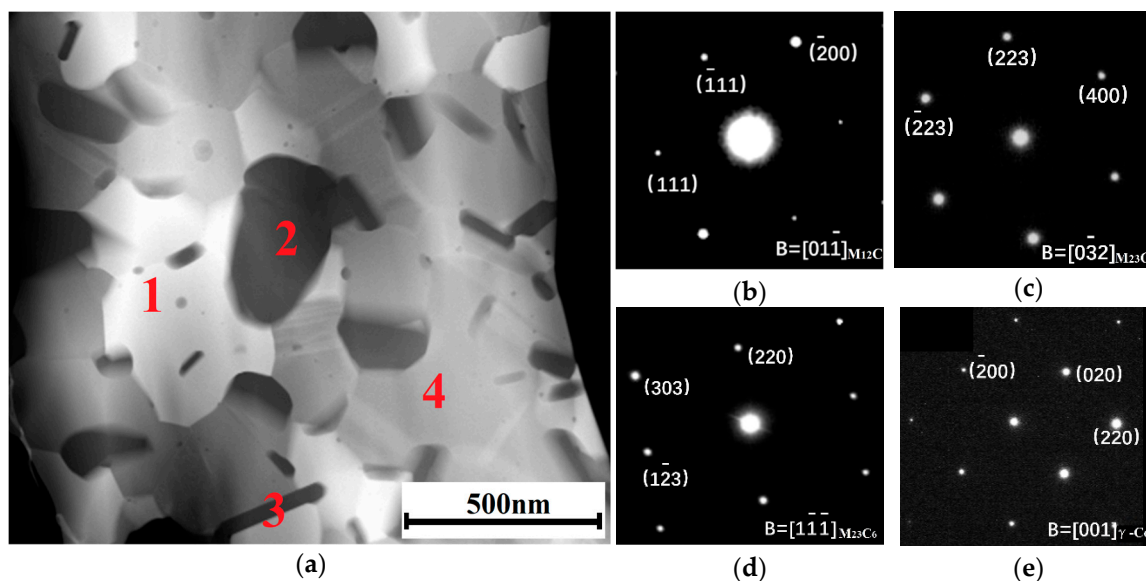


Figure 5. STEM high-angle annular dark field (HAADF) image of the obtained bulk cobalt-based alloy (a) and selected area electron diffraction (SAED) patterns of the different phases labeled in (a), (b) point 1, bright, (c) point 2, dark, (d) point 3, dark, and (e) point 4, grey.

Table 1. STEM-EDS results of the phases in the prepared bulk cobalt-based alloy (at. %).

Point	Cr	W	V	Ni	Co	Fe	C	Phase
1 (bright)	29.93	16.44	8.11	0	31.40	2.11	12.01	$M_{12}C$
2 (dark)	50.46	0	23.38	0	0	0	21.52	$M_{23}C_6$
3 (dark)	53.08	0	26.07	0	0	0.70	17.39	$M_{23}C_6$
4 (grey)	25.20	1.96	2.64	6.33	55.08	4.33	4.46	$\gamma-Co$

Interestingly, the TEM bright field image of the prepared bulk cobalt-based alloy (Figure 6) showed a large number of nano-twins in the $\gamma-Co$ matrix. The thickness of twin lamellae varied between 10–60 nm.

The alloy had a high hardness of the 960 ± 9.2 HV5. Figure 7 shows the indentation morphology of the Vickers hardness test and the crack produced by the hardness indentation showing the fracture of $M_{12}C$ and $M_{23}C_6$ -type carbide particles as well as the plastic deformation of $\gamma-Co$ matrix, marked by arrows A, B, and C in the Figure 7b, respectively. Only a very short crack was found revealing that the prepared bulk alloy has a good toughness. According to the indentation methods for determining toughness, the fracture toughness K_{Ic} of the alloy was about 10.5 ± 0.46 MPa·m^{1/2} calculated by the Equation (1) [15]:

$$K_{Ic} = \delta(E/H)^{1/2}(P/a^{3/2}), \quad (1)$$

where, δ is a geometrical factor, for a Vickers indentation $\delta = 0.016$; E is the Young's modulus, according to Ahmed's report [7], $E = 320$ GPa was selected in Equation (1); H is the hardness of the sample, $H = 960$ HV = 9.4 GPa; $2a$ is the crack size along the diagonal of the indentation, $2a = 115.2 \pm 3.4$ μ m; P is the load for Vickers indentation, $P = 49$ N.

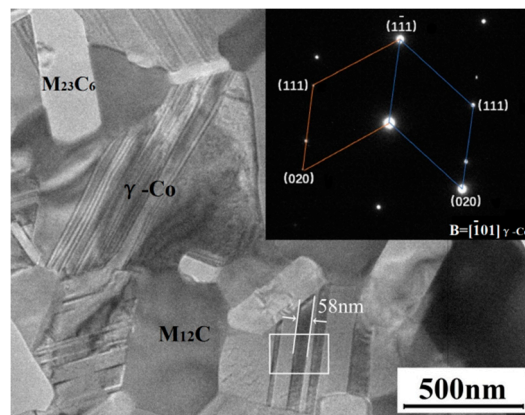


Figure 6. TEM bright field image of the sintered cobalt-based alloy showing a large number of nano-twins in the γ -Co matrix. Inlet is the SAED pattern for the marked area.

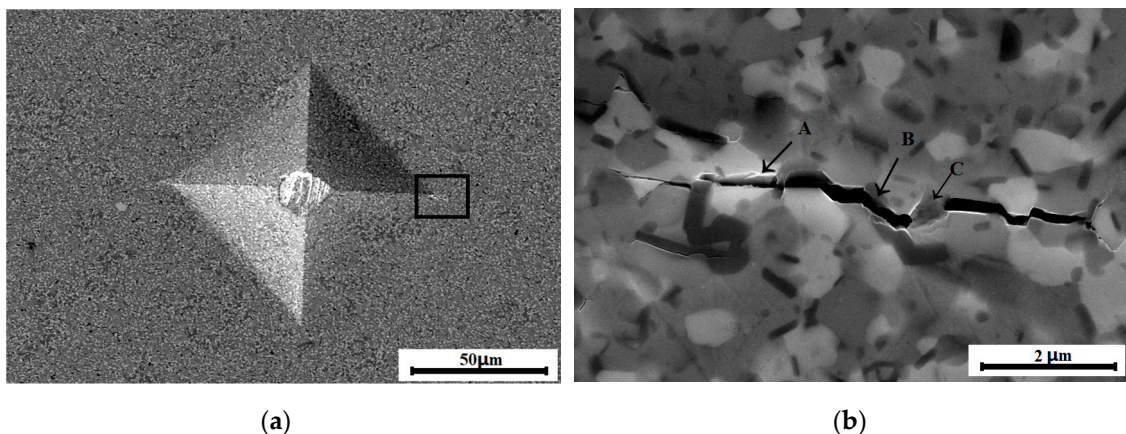


Figure 7. The indentation morphology of the Vickers indentation (a) and the crack generated by the indentation (b).

4. Discussion

The common cobalt-based alloy carbides are M_7C_3 , $M_{23}C_6$, M_6C , MC , etc. Service or aging at elevated temperature causes a large amount of secondary carbides, such as M_6C and $M_{23}C_6$ [16]. In the present study, the prepared alloy had M_6C and $M_{23}C_6$ -type carbides (Figure 4). The vanadium was mainly distributed in $M_{23}C_6$ -type carbide in the prepared cobalt-based alloy, as shown in Table 1, instead of forming V-rich MC-type carbide. Even though vanadium is a strong MC-type carbide-forming or MX-type (M indicates metal elements, X indicates carbon or nitrogen) carbonitride-forming element, V-rich MC-type carbide is not found in the prepared bulk cobalt-based alloy with 5 wt. % V. However, MX-type precipitate is usually found in 9-12Cr-type martensitic/ferritic heat resistant steel with much less V content of 0.2 wt. % [17,18]. The microstructural characteristics of the prepared alloy is that the $M_{12}C$ -type carbide particles and coarse $M_{23}C_6$ -type carbide particles are distributed in the γ -Co matrix in which there are a large number of nano-twins, and fine $M_{23}C_6$ -type carbide particles present within both the γ -Co matrix and $M_{12}C$ -type carbide particles (Figure 3).

According to the results mentioned above, the microstructure formation mechanism of the prepared bulk cobalt-based alloy can be illustrated as shown in Figure 8. During the heating and hot pressed sintering process, the mechanically alloyed powders transform from an amorphous state with some nano-sized W particles to γ -Co supersaturated solid solution, then the $M_{12}C$ -type and coarse $M_{23}C_6$ -type carbides are formed as follows: $23(Cr, V) + 6C \rightarrow (Cr, V)_{23}C_6$ and $12(W, Cr, Co, V) + C \rightarrow (W, Cr, Co, V)_{12}C$ [19]. Finally, the fine $M_{23}C_6$ -type carbide particles within both the γ -Co matrix and $M_{12}C$ -type carbide particles are precipitated from the γ -Co matrix and $M_{12}C$ -type carbide during the furnace cooling process after hot pressed sintering because their size is much smaller than that of the

striplike $M_{23}C_6$ carbide. $M_{23}C_6$ carbide usually precipitates along grain boundaries during the cooling process in conventional alloys, such as austenitic steels and Ni-based superalloys. While the fine $M_{23}C_6$ carbide precipitates within γ -Co matrix in the present V-containing alloy, we think the reason might be that the $M_{23}C_6$ carbide contained a lot of V which has a larger atom size and lower diffusion coefficient than Cr resulting in nucleation of $M_{23}C_6$ within γ -Co matrix and growing up slowly.

The nominal composition of the alloy in atomic fraction was 35.8% Co, 40.1% Cr, 8.9% W, 5.5% Ni, 6.4% V, 3.2% C. From the STEM-EDS data as shown in Table 1, it can be seen that almost all W was distributed in $M_{12}C$, almost all V in $M_{23}C_6$ and the atomic fraction of Cr in $M_{23}C_6$ is about two times the atomic fraction of V. Based on the STEM-EDS data, the formation of $M_{12}C$ and $M_{23}C_6$ may consume about 6.1% C in atomic fraction, much more than the added 3.2% C. In fact, the carbon content in the prepared alloy was determined to be 1.9% in weight fraction, i.e., 9.8% in atomic fraction by a carbon and sulfur analyzer. The stainless-steel vial and stainless-steel balls were used to prepare the Co-based alloy powders in this work. According to the STEM-EDS results, only a small amount of Fe was indeed introduced into the sintered alloy, it is impossible that the carbon introduced from the stainless-steel vial and stainless-steel balls have much influence. The excess carbon may come from graphite mold during used for hot pressed sintering and causes an increase in amount of carbides.

The mechanism of nano-twins formation in the prepared cobalt-based alloy is not fully understood yet. Twins are common in metals with a FCC structure because of low stacking fault energy [20,21]. Twins are usually formed by sliding a single crystallographic dislocation on a continuous $\{111\}$ plane driven by a Peach-Koehler force [22]. However, there is no report about the existence of large amounts of nano-twins in a cobalt-based alloy. From a thermodynamic point of view, the formation of twins decreases the total interfacial energy, because the excess energy for coherent twin boundaries (TB) is much smaller than that for conventional high angle grain boundaries (GB). Twins prefer to nucleate at GBs or triple junctions (TJ) to reduce the GB energies by means of the twinning-induced orientation change. Although an extra TB is formed, the sum of the interfacial energies (including GBs and TBs) will be reduced by twinning [23]. In the prepared alloy, the lattice constants of $M_{12}C$ and $M_{23}C_6$ carbides were 1.0922 nm and 1.0657 nm, respectively, about three times the γ -Co lattice constant (0.3552 nm) calculated using XRD data. Therefore, the interface between γ -Co and carbides are prone to form coherent interfaces, which causes a large lattice stress and increases the interfacial energy. In order to reduce the interfacial energies, a large number of nano-twins are formed in the γ -Co matrix.

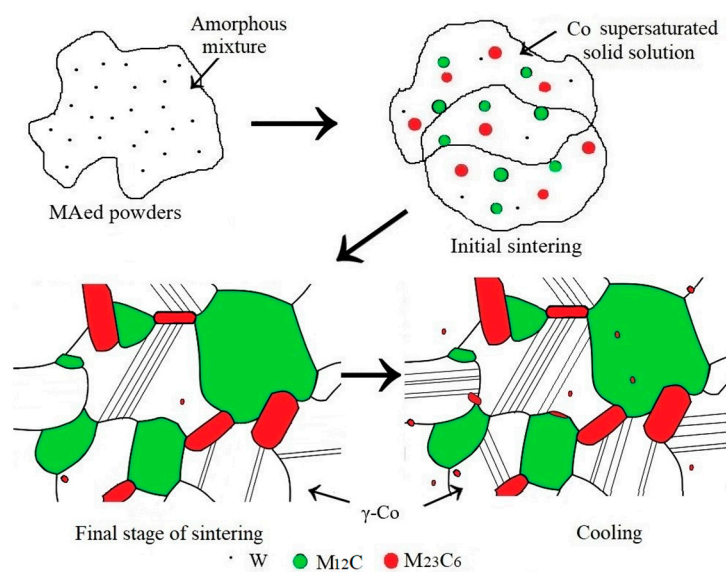


Figure 8. Schematic illustration of the microstructure evolution of cobalt-based alloy during hot pressing sintering and cooling.

The hardness of the prepared bulk cobalt-based alloy was up to 960 ± 9.2 HV5. Casas et al. [11] reported that the prepared ternary and quinary cobalt-based superalloys by field assisted sintering techniques have a hardness of about 650 and 900 HV, respectively. Ahmed [7] used Re-Hot Isostatic Pressing to prepare Stellite 20 alloy with a hardness of 650 HV. Compared with these reported results, the hardness of the prepared cobalt-based alloy in this work was increased significantly. It is reported that a Triballoy T800 alloy coating has a hardness up to 1000 HV, however, the brittle nature of Laves phases causes a low fracture toughness and reduces the performance of T800 alloy in a wide range of applications where other properties such as certain ductility and fracture toughness are also needed [24]. The high hardness depends on the microstructure. A large amount of fine carbide dispersed uniformly in the prepared cobalt-based alloy, which served as a reinforcement agent. Carbides distributed at the γ -Co grain boundaries prevent slipping and migration of grain boundaries and inhibit grain growth. Carbides inside the γ -Co grains block dislocation movements to enhance the matrix. The W alloying element added in the cobalt based alloy was as high as 25%, which means that more W-containing $M_{12}C$ carbide in the prepared alloy can effectively improve the hardness, more than in a common cobalt based alloy [25]. In addition, many nano-twins are also found in the γ -Co matrix, which also play an important role in strengthening the matrix by blocking the dislocation motion [26,27], further enhancing the hardness. This is also the main difference in the reinforcement mechanism compared with the previously studied cobalt-based alloys [28]. Therefore, under the synergistic effect of solid solution strengthening, dispersion strengthening and nano-twins, the as-prepared cobalt-based alloy presents high hardness. Moreover, the matrix of the prepared Cobalt-based alloy is γ -Co with a FCC structure and has a fine grain structure. The crack propagation can be restrained by the plasticity of γ -Co matrix as shown in Figure 7 marked with arrow C. Therefore, the prepared cobalt-based alloy had not only high hardness but also good toughness, and a good wear-resistant property of the alloy can be expected.

5. Conclusions

In summary, a bulk V-containing cobalt-based alloy with high chromium and tungsten contents was prepared by mechanical alloying and hot pressed sintering using Co, Cr, W, Ni, V, and C pure element powders, the following can be concluded:

- (1) All elements can be mixed uniformly while Co, Cr, and Ni elements are made into an amorphous state after 10h ball milling in a high energy ball miller.
- (2) The microstructure of the prepared alloy was composed of γ -Co matrix with a large number of nano-twins and fine $M_{23}C_6$ and $M_{12}C$ carbide particles which were well-distributed in the alloy. The V element was mainly distributed in $M_{23}C_6$ -type carbide and no V-rich MC-type carbide is found in the microstructure.
- (3) The prepared alloy had a high hardness up to 960 ± 9.2 HV5 and good fracture toughness K_{Ic} of about 10.5 ± 0.46 MPa·m^{1/2}.
- (4) The high hardness was mainly attributed to the synergistic effect of solid solution strengthening, dispersion strengthening, and the large number of nano-twins.

Author Contributions: Conceptualization, N.L.; methodology, N.L. and F.Y.; validation, N.L.; formal analysis, F.Y. and L.F.; writing—original draft preparation, N.L.; writing—review and editing, L.F.

Funding: This research was funded by the natural science foundation of Shandong province (Grant Number: ZR2016EMM01).

Acknowledgments: This work was supported by the natural science foundation of Shandong province (Grant Number: ZR2016EMM01). The authors are grateful for the assistance from Jinye Niu.

Conflicts of Interest: The authors declare no conflict of interest.

References

1. Petersson, A.; Ågren, J. Constitutive behaviour of WC–Co materials with different grain size sintered under load. *Acta Mater.* **2004**, *52*, 1847–1858. [[CrossRef](#)]
2. Mingard, K.P.; Roebuck, B.; Marshall, J.; Sweetman, G. Some aspects of the structure of cobalt and nickel binder phases in hardmetals. *Acta Mater.* **2011**, *59*, 2277–2290. [[CrossRef](#)]
3. Jiang, K.; Liu, R.; Chen, K.; Liang, M. Microstructure and tribological properties of solution-treated Tribaloy alloy. *Wear* **2013**, *307*, 22–27. [[CrossRef](#)]
4. Xu, W.; Liu, R.; Patnaik, P.C.; Yao, M.X.; Wu, X.J. Mechanical and tribological properties of newly developed Tribaloy alloys. *Mater. Sci. Eng. A* **2007**, *452–453*, 427–436. [[CrossRef](#)]
5. Sun, S.H.; Koizumi, Y.; Kurosu, S.; Li, Y.P.; Matsumoto, H.; Chiba, A. Build direction dependence of microstructure and high-temperature tensile property of Co–Cr–Mo alloy fabricated by electron beam melting. *Acta Mater.* **2014**, *64*, 154–168. [[CrossRef](#)]
6. Cordero, M.C.; Srinivasarao, B.; Campos, M.; Junceda, A.G.; Torralba, J.M. On the role of processing parameters in sintered new Co-based (W,Al) alloys. *J. Alloys Compd.* **2016**, *674*, 406–412. [[CrossRef](#)]
7. Ahmed, R.; Lovelock, H.L.V.; Davies, S.; Faisal, N.H. Influence of Re-HIPing on the structure–property relationships of cobalt-based alloys. *Tribol. Int.* **2013**, *57*, 8–21. [[CrossRef](#)]
8. You, X.H.; Wang, G.G.; Wang, J.; Xu, T.; Zhang, H.Y.; Wei, H. Effect of solid solution treatment on microstructure and mechanical properties of hot-press CoCrW alloys. *Acta Metall. Sin.* **2016**, *52*, 161–167.
9. Hou, J.; Dong, J.X.; Yao, Z.H.; Jiang, H.; Zhang, M.C. Influences of PPB, PPB affect zone, grain boundary and phase boundary on crack propagation path for a P/M superalloy FGH4096. *Mater. Sci. Eng. A* **2018**, *724*, 17–28. [[CrossRef](#)]
10. Zhang, L.; Qu, X.H.; He, X.B.; Din, R.; Qin, M.L.; Zhu, H.M. Hot deformation behavior of Co-base ODS alloys. *J. Alloys Compd.* **2012**, *512*, 39–46. [[CrossRef](#)]
11. Casasa, R.; Gálvez, F.; Campos, M. Microstructural development of powder metallurgy cobalt-based superalloys processed by field assisted sintering techniques (FAST). *Mater. Sci. Eng. A* **2018**, *724*, 461–468. [[CrossRef](#)]
12. Ren, F.Z.; Zhu, W.W.; Chu, K.J. Fabrication, tribological and corrosion behaviors of ultra-fine grained Co–28Cr–6Mo alloy for biomedical applications. *J. Mech. Behav. Biomed. Mater.* **2016**, *60*, 139–147. [[CrossRef](#)] [[PubMed](#)]
13. Berthod, P.; Khair, M. Thermodynamic and experimental study of cobalt-based alloys designed to contain TiC carbides. *Calphad* **2016**, *60*, 34–41. [[CrossRef](#)]
14. Burton, A.W.; Ong, K.; Rea, T.; Chan, I.Y. On the estimation of average crystallite size of zeolites from the Scherrer equation: A critical evaluation of its application to zeolites with one-dimensional pore systems. *Microp. Mesop. Mater.* **2009**, *117*, 75–90. [[CrossRef](#)]
15. Meyers, M.A.; Chawla, K.K. *Mechanical Behavior of Materials*; Cambridge University Press: Cambridge, UK, 2009; p. 549.
16. Yang, F.M.; Sun, X.F.; Zhang, W.; Kang, Y.P.; Guan, H.R.; Hu, Z.Q. Secondary M₆C precipitation in K40S cobalt-base alloy. *Mater. Lett.* **2001**, *49*, 160–164. [[CrossRef](#)]
17. Zhang, C.; Cui, L.; Wang, D.P.; Liu, Y.C.; Liu, C.X.; Li, H.J. The heterogeneous microstructure of heat affect zone and its effect on creep resistance for friction stir joints on 9Cr–1.5W heat resistant steel. *Scrip. Mater.* **2019**, *158*, 6–10. [[CrossRef](#)]
18. Wang, H.; Yan, W.; Zwaag, S.; Shi, Q.Q.; Wang, W.; Yang, K.; Shan, Y.Y. On the 650 °C thermostability of 9–12Cr heat resistant steels containing different precipitates. *Acta Mater.* **2017**, *134*, 143–154. [[CrossRef](#)]
19. Jiang, W.H.; Yao, X.D.; Guan, H.R.; Hu, Z.Q.; Jiang, W.H. Secondary carbide precipitation in a directionally solidified cobalt-base superalloy. *Metall. Mater. Trans. A* **1999**, *30*, 513–520. [[CrossRef](#)]
20. Szczerba, M.J.; Kopacz, S.; Szczerba, M.S. Experimental studies on detwinning of face-centered cubic deformation twins. *Acta Mater.* **2016**, *104*, 52–61. [[CrossRef](#)]
21. Mahajan, S. Critique of mechanisms of formation of deformation, annealing and growth twins: Face-centered cubic metals and alloys. *Scrip. Mater.* **2013**, *68*, 95–99. [[CrossRef](#)]
22. Gu, J.; Zhang, L.X.; Ni, S.; Song, M. Formation of large scaled zero-strain deformation twins in coarse-grained copper. *Scrip. Mater.* **2016**, *125*, 49–53. [[CrossRef](#)]

23. Lu, L.; Shen, Y.F.; Chen, X.H.; Qian, L.H.; Lu, K. Ultrahigh Strength and High Electrical Conductivity in Copper. *Science* **2004**, *304*, 422–425. [[CrossRef](#)]
24. Tobar, M.J.; Amado, J.M.; Álvarez, C.; García, A.; Varela, A.; Yáñez, A. Characteristics of Tribaloy T-800 and T-900 coatings on steel substrates by laser cladding. *Surf. Coat. Technol.* **2008**, *202*, 2297–2301. [[CrossRef](#)]
25. Lu, Y.J.; Wu, S.Q.; Gan, Y.L.; Li, J.L.; Zhao, C.Q.; Zhuo, D.X.; Lin, J.X. Investigation on the microstructure, mechanical property and corrosion behavior of the selective laser melted CoCrW alloy for dental application. *Mater. Sci. Eng. C* **2015**, *49*, 517–525. [[CrossRef](#)] [[PubMed](#)]
26. Liu, Y.Q.; Zhou, J.Q. The fatigue crack growth in hierarchically nano-twinned materials. *Eng. Fract. Mech.* **2018**, *204*, 63–71. [[CrossRef](#)]
27. Zhu, Y.T.; Liao, X.Z.; Wu, X.L. Deformation twinning in nanocrystalline materials. *Prog. Mater. Sci.* **2012**, *57*, 1–62. [[CrossRef](#)]
28. Corderoa, M.C.; Campos, M.; Freund, L.P.; Kolb, M.; Neumeier, S.; Göken, M.; Torralba, J.M. Microstructure and compression strength of Co-based superalloys hardened by γ' and carbide precipitation. *Mater. Sci. Eng. A* **2018**, *734*, 437–444. [[CrossRef](#)]



© 2019 by the authors. Licensee MDPI, Basel, Switzerland. This article is an open access article distributed under the terms and conditions of the Creative Commons Attribution (CC BY) license (<http://creativecommons.org/licenses/by/4.0/>).